Research Article | Vol. 29, No. 7 / 29 March 2021 / Optics Express 10853
Optics EXPRESS

Vibration monitoring based on optical sensing of mechanical nonlinearities in glass suspended waveguides

ENRICO CASAMENTI,* TAO YANG, PIETER VLUGTER, AND YVES BELLOUARD

Galatea Laboratory, IMT/STI, Ecole Polytechnique Fédérale de Lausanne (EPFL), Rue de la Maladière 71b, CH - 2000 Neuchâtel, Switzerland
enrico.casamenti@epfl.ch

Abstract: Vibration monitoring plays a key role in numerous applications, including machinery predictive maintenance, shock detection, space applications, packaging-integrity monitoring and mining. Here, we investigate mechanical nonlinearities inherently present in suspended glass waveguides as a means for optically retrieving key vibration pattern information. The principle is to use optical phase changes in a coherent light signal travelling through the suspended glass waveguide to measure both optical path elongation and stress build-up caused by a given vibration state. Due to the intrinsic non-linear mechanical properties of double-clamped beams, we show that this information not only offers a means for detecting excessive vibrations but also allows for identifying specific vibration patterns, such as positive or negative chirp, without the need for any additional signal processing. In addition, the manufacturing process based on femtosecond laser exposure and chemical etching makes this sensing principle not only simple, compact and robust to harsh environments but also scalable to a broad frequency range.

1. Introduction

Natural or anthropogenic, mechanical vibrations contain a wealth of information concerning the state of dynamically evolving systems as well as structural health conditions of passive structures. For instance, in rotating machinery, occurrences of unexpected vibration patterns are key indicators of wear, failure or inappropriate machining parameters when considering manufacturing applications. Particularly interesting for predictive maintenance, vibration monitoring can be essential for systems operating in harsh and/or EM-sensitive environments such as space applications or simply for machines subject to lightning or strongly and rapidly varying weather conditions, like in the case of wind turbines blades [1–4], where failures can produce catastrophic consequences. Beyond machinery, there are countless examples and situations, from seismic activities to structural health monitoring (SHM) where proper monitoring of vibrations is essential.

Popular solutions for vibration monitoring (see for instance the reviews [1,5,6]) - can be sub-divided into three main categories: electrical transducers (piezoelectric, strain gauges, accelerometers, etc.), optical fibers (Fiber-Bragg-Gratings, exploiting Raman or Brillouin scattering, interferometers, strain fibers, etc.) or simply vision-based contact-less methods, when structures are large enough and when observations conditions permit it [7,8]. Among these solutions, fiber-based ones are the most adapted to harsh conditions, such as extreme temperatures, and electromagnetic (EM) sensitive environment and can easily be scaled up and multiplexed. However, they require costly and sophisticated emitters and processing units.

Here, we explore a different concept of vibration monitoring sensor that combines intrinsic non-linear mechanical properties with a simple interferometric optical read-out method.

#414191 https://doi.org/10.1364/OE.414191
Journal © 2021 Received 18 Nov 2020; revised 8 Mar 2021; accepted 10 Mar 2021; published 23 Mar 2021

Optics EXPRESS

The working principle, illustrated in Fig. 1, consists of using a suspended double-clamped transparent beam that, once vibrating, induces a phase modulation in a coherent optical wave travelling through and that remains confined within the glass structure.

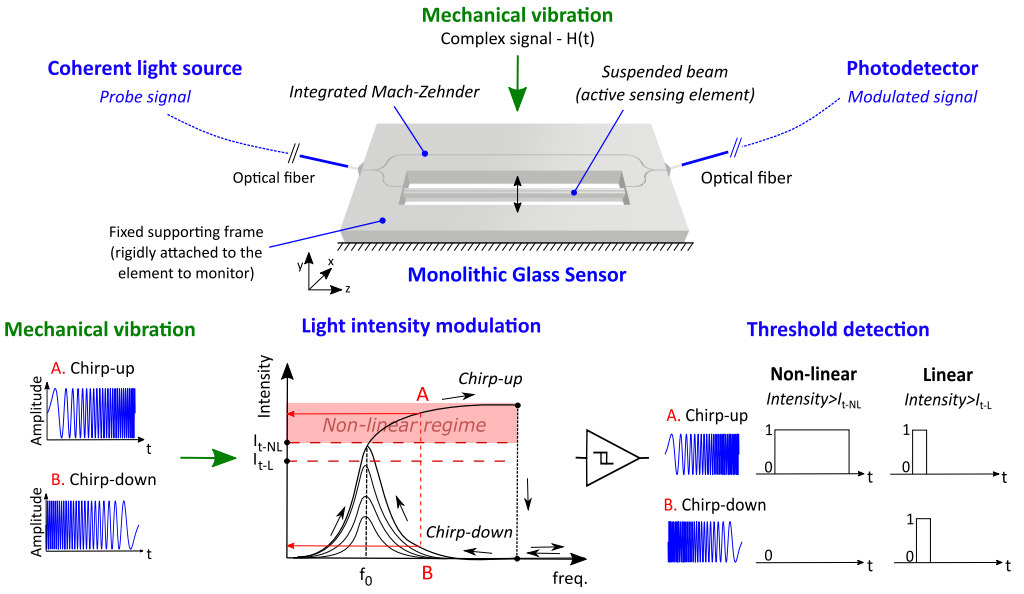

Fig. 1. Device concept and working principle. The oscillation of a suspended transparent double-clamped beam is excited by the mechanical vibrations of the monitored device. The oscillations cause the coherent light travelling through the beam to undergo phase-modulation with an intensity that depends not only on the frequency of excitation, but also on its previous state, i.e. chirp-up or chirp-down. Consequently, depending on the frequency sweeping direction, two different states of oscillations amplitude - and in turn modulation - (A and B) are reached and can be readily sensed by a photodetector. The bottom right schematic illustrates an example of use with an intensity-threshold detection scheme and compares a non-linear and a linear case. Here "0" and "1" represent two states, appropriately chosen, to monitor. In the non-linear case, the state "1" corresponds to the detection of a frequency chirp-up (intensity above I_{t-NL}); while in the linear case the state "1" (intensity above I_{t-L}) is reached for both chirp-up and –down.

Being mechanically over-constrained, the double-clamped beam, when excited at high amplitudes, exhibits a signature hysteresis in the frequency domain [9–12]. At high excitation amplitudes, when the frequency sweeps up, the resonant peak survives over a large frequency window, effectively enlarging its spectral range, while upon sweeping down, a different frequency-amplitude response path is observed. Consequently, the device oscillatory state depends on whether it was previously exposed to a vibrations frequency increase or decrease.

In the context of sensing, this *intrinsic* property is particularly interesting and offers a means to embed 'intelligence' in the system without adding signal-processing complexity. By injecting light in the transparent beam, we transduce this mechanical non-linearity *directly* into the optical domain. In fact, not just the oscillations amplitude, but also the phase-shift induced to the travelling optical wave depends on the previous frequency state.

This nonlinearity enables *direct* sensing of dynamic vibrational states, such as a chirp-up or a chirp-down, with no signal post-processing required, as opposed to conventional vibration sensors [13,14]. In fact, those vibrational states result in two clearly distinct points in the frequency-amplitude characteristic response (see points A and B in Fig. 1). By exploiting such property, one can achieve *embedded* monitoring of complex dynamic states, as for example the

Optics EXPRESS

start and stop of a rotatory engine or vibrations due to a propagating shock pulse. For example, after the start, an engine reaches its working speed performing a sweep-up in frequency due to inherent vibrations of the solid body. In general, the designer of such an engine will ensure that the vibrations of the hull are minimal, which corresponds to a healthy state of the system. Suppose now that due to wear or other unwanted causes (e.g. environmental disturbances) the vibrations level increases dramatically during the sweeping-up phase. The sensor will then enter a non-linear regime where it should normally not be if the machine were under proper operation and in a healthy state. As a result, the monitored signal can be used to ring an alarm that something is malfunctioning in the start-up of the engine, which is often a critical phase.

Such a vibrations sensor requires just a low-cost coherent light source and a photodetector as external components that can be positioned at an arbitrarily remote distance from the sensing element using optical fibers. Inherently simple, this principle can be scaled in dimensions and number of sensing devices. The monolithic glass sensing results in high optical efficiency, which lowers the requirements for both light-source power and photodetector sensitivity. In practice, the sensing element is made out of a fused silica substrate, thanks to femtosecond laser exposure combined with chemical etching. This results in a sensing element immune, not only, to EM radiations, but also to a majority of corrosive environments and that can survive temperatures, typically up to 600 °C [15] – a temperature above, which waveguides may start fading. The operating bandwidth is selected by design of the vibrating beam and can vary from few tens of Hz to tens of kHz. Furthermore, in another work, we demonstrated that the non-linear frequency response pattern of a double-clamped fused silica beam can be shaped from hardening to softening or even linearized, through laser re-exposure of the vibrating element, offering an additional degree of freedom for tuning the dynamic response of the sensor [12]. As an illustration of a possible use, re-exposing the vibrating beam could be used to switch the intensity-threshold detection scheme shown in Fig. 1 from a chirp-up to a chirp-down frequency pattern detector.

2. Proof-of-concept: fabrication, modelling and measurement setup

Through its oscillations, the suspended beam modulates the phase of an optical wave travelling through it due to the effective change in optical path-length as well as the stress-induced in the beam while deforming. Due to its clamped-clamped boundary conditions, the beam has an intrinsic non-linear dynamical behavior. As the beam deflects, a tension proportional to the beam deflection arises. This dynamical behavior is modeled using Duffing-oscillator formalism [16], which leads to the following harmonic equation:

$$\frac{d^2y(t)}{dt^2} + 2\delta\frac{dy(t)}{dt} + \alpha_1 y(t) + \alpha_2 y^2(t) + \alpha_3 y^3 = H(t). \tag{1}$$

where $y(t)$ is the vertical displacement, 2δ is a dissipation term, $H(t)$ is the mechanical vibration to monitor, and α_1, α_2 and α_3 are the linear, quadratic and cubic mass-normalized nonlinear stiffness coefficients, respectively.

To investigate the sensor dynamic response over a broad frequency range, we specifically designed a suspended double-clamped beam placed in a V-shaped cavity out of a single piece of fused silica, benefiting from the three-dimensional capability of the manufacturing process used here. This process (described in [17]) consists first, in exposing the material to femtosecond laser radiation, and second, in etching the laser-exposed region in a low-concentration chemical bath. The beam is set into vibration using dielectrophoresis - a second-order electrostatic effect that can be used to induce a force-field on a dielectric object, as demonstrated elsewhere [16,18]. The beam rectangular cross-section defines a fundamental vibration mode along the y-axis as defined in Fig. 1 and Fig. 2.

Optics EXPRESS

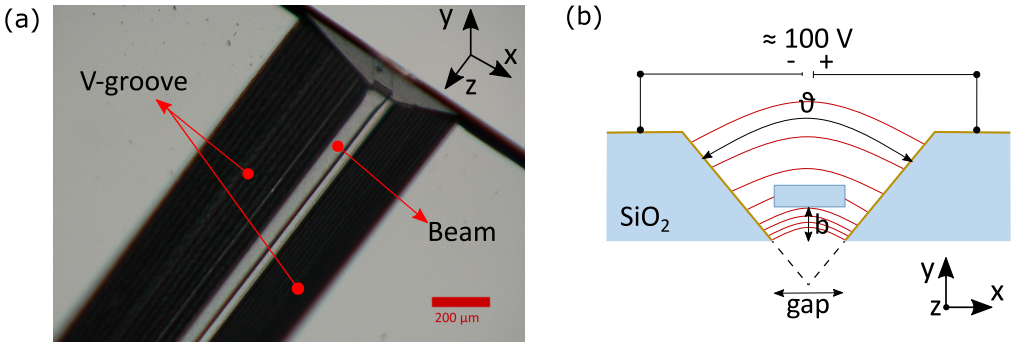

Fig. 2. (a) Optical microscope picture showing one side of the prototype before covering the V-groove with a gold layer. (b) Cross-section and key design parameters used to optimize dielectrophoresis-based actuation. The yellow lines represent gold electrodes. Considering the rectangular beam cross-section, its fundamental vibration mode occurs along the y- axis.

To fabricate the device, we exposed the volume-to-be-removed to a Ytterbium-fiber amplifier laser emitting 270 fs pulses at a repetition rate of 800 kHz, with a pulse energy of 240 nJ. The laser is focused using a 0.4-numerical aperture objective down to a waist of approximately 1.5 µm. The substrate used is UV-grade fused silica (Corning 7980 0F), 500 µm-thick, and 25 mm-square. Following laser exposure, the specimen is etched in a 2.5%-HF acid bath for several hours, a step during which, laser-exposed regions are dissolved. In the present study, the beam is 23 mm-long and has a 50×100 µm^2 cross-section. A final step of CO_2-laser polishing is implemented to achieve optical surface quality, and in turn, to limit scattering losses [19].

Finally, a thin gold layer is sputter-deposited on the V-groove to form two electrodes, while a 3D glass mask prevents the deposition of gold on the beam itself. As such, the double-clamped beam dimension defines a multi-mode waveguide. However, the working principle is down scalable to single-mode operation, albeit operating in a different frequency range. Otherwise, single-mode operation with the present double-clamped beam dimension can be achieved by femtosecond waveguide writing [20,21].

In earlier works, we modelled freestanding and double-clamped beams under dielectrophoresis (DEP) actuation (see T. Yang *et al.* [12,17]). Using the same design optimization framework (Fig. 2(b)), we selected $b = 50$ µm, gap $= 120$ µm and $\theta = 90°$ as optimal design parameters in this particular case. In a static excitation case, comparing the DEP actuation magnitude with the nonlinear elastic restoring force, we calculated a deflection of about 1 µm with a driving voltage close to 100 V^{dc}. From Euler-Bernoulli beam-theory and by solving the equation of motion of a double-clamped beam in free oscillations, the predicted first natural frequency $f_1 = 610$ Hz is found. For these calculations and in the sequel, both curviness and initial beam tension that may occur as a byproduct of the CO_2 exposure are neglected. The density and Young's modulus are taken as 2200 kg/m^3 and 72.5 GPa, respectively.

A signal generator combined with an amplifier is used to set the beam into vibrations. To monitor the beam displacement peak-amplitude, a laser triangulation sensor (Keyence LK-H022K) is focused at the center and mid-length of the suspended beam. The dynamic behavior is investigated through a series of frequency sweep-cycles around the first resonance mode. A 632 nm-HeNe laser is injected in the suspended waveguide using standard free-space optics and collected using a microscope objective. Phase-shifts in the optical signal due to the beam deflection are measured using a Mach-Zehnder interferometer (MZI) (see Fig. 3). Note that the wavelength is chosen for the sake of experimental commodity, but any wavelength within the transparency window of fused silica can be used.

Optics EXPRESS

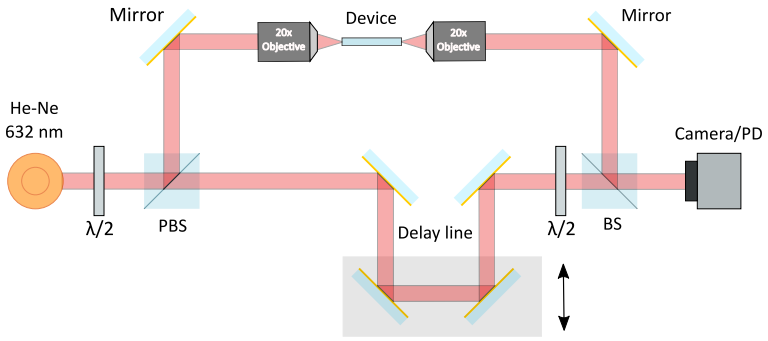

Fig. 3. Schematic of the Mach-Zehnder interferometer setup used for the optical phase shift measurements of our proof-of-concept experiment.

A delay line is arranged to compensate for the difference in path lengths between the two arms. In addition, a half-wave plate is used in combination with a polarized beam splitter (PBS) to control the distribution of light intensity between the two arms. At last, a standard CMOS camera (Thorlabs DCC1645C) and a photodetector (Thorlabs PDA36A-EC) are used for alignment and to measure the intensity of the recombined light beam, respectively. Finally, the photodetector signal, together with the displacement sensor measurement and the applied excitation voltage are collected with a DAQ. It should be noticed that the MZI itself can be further integrated by direct writing in the same fused silica substrate containing the vibrating beam, as demonstrated elsewhere (see for example [22]), to obtain a combination of mechanical functions and waveguides exploiting the different modifications induced by femtosecond lasers [23,24].

3. Experimental results

Figure 4(a) shows the beam vibration amplitude for upwards deflections as a function of frequency and DEP input voltage. The first natural frequency peak (along the y-axis in Fig. 2) is measured at 613 Hz for 100 V continuous voltage with a 25 V peak-to-peak oscillation added to it. The second main frequency vibration mode (lateral, i.e. along the x-axis in Fig. 2) is found at 815 Hz. The continuous voltage polarizes the dielectrics, while the oscillating voltage generates the excitation force that sets the beam into vibrations. For increasing amplitudes of oscillations, the difference in behavior between sweeping up or down in frequencies becomes more pronounced, eventually exhibiting a hysteresis, characteristic of a typical 'hardening' behavior. Increasing the excitation voltage up to 50 V_{pp}, a maximum displacement of more than 50 µm is found at mid-length of the suspended beam. The maximum oscillation amplitude is set by the flexural strength of the material. For example, assuming a flexural strength of 1 GPa, which remains a conservative value [25], one can calculate a maximum deflection of ≈ 200 µm at mid length, for the dimensions used here, corresponding to about 0.87% of the beam length. No change is recorded for the Q-factor, which remains around 50 in standard laboratory conditions (i.e. T = 25 °C and atmospheric pressure).

To explore the coupling of the mechanical nonlinearity with the optical modulation, the same set of actuating voltages used in Fig. 4(a) is applied to the device, but this time the collected output is the optical intensity-modulated signal, then converted in retardance. The results are shown in Fig. 4(b). As expected, strong similarities with the nonlinear behavior of the beam-displacement amplitude shown in Fig. 4(a) are observed and manifest themselves by a difference in both, amplitude and frequency, visible while sweeping towards higher or lower frequencies.

Optics EXPRESS

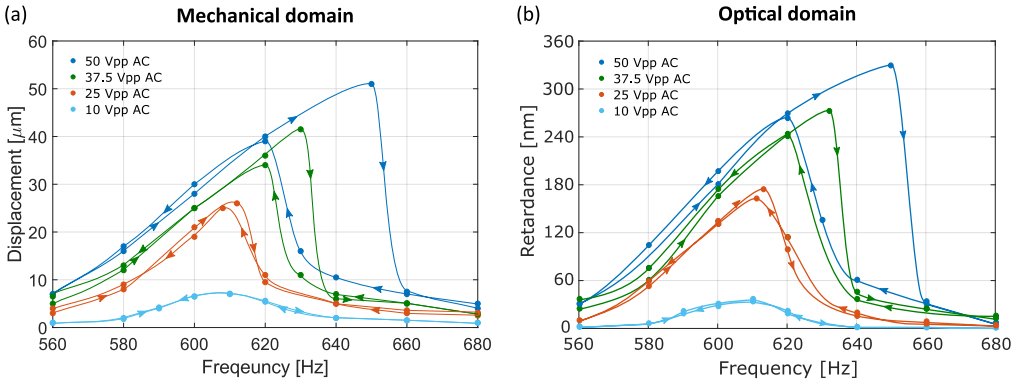

Fig. 4. Nonlinear dynamic response of the double-clamped beam actuated by dielectrophoresis. The device is under a 100 V static voltage onto which an oscillating voltage of varying intensity is superposed in order to set the beam in vibration. Dynamic behaviors for both sweeping -up and -down in frequency are shown, exhibiting a strong hysteresis and hardening behavior. (a) In the mechanical domain, the displacement corresponding to the upward deflection of the double-clamped beam as measured by the laser triangulation sensor is shown. (b) In the optical domain, the intensity signal from the photodetector is converted in retardance and taken as response. Displacement error measurement is +/- 0.1 μm, while the frequency error measurement is estimated to be +/- 2 Hz and the retardance one to +/- 10 nm. The curves are drawn as visual aids.

To correlate the displacement to the retardance and therefore, to couple the mechanical domain to the optical one, a simple model accounting for the beam elongation is implemented and to it we add the contribution purely related to the stress developing in the beam.

From the measured displacement, we calculate the corresponding elongation of the double-clamped beam. We consider an equivalent, uniformly distributed load that would induce the measured deflection. Under these conditions and by considering that the deflections are very small (three orders of magnitude lower than the double-clamped beam length), we can use the classical Euler-Bernoulli beam theory and write the beam profile for a downwards deformation as:

$$y(z) = \frac{P}{24EJ_x}(-z^4 + 2Lz^3 - L^2z^2). \tag{2}$$

Where $y(z)$ is the vertical displacement, E is the Young modulus of fused silica, $J_x = t^3w/12$ is the second moment of inertia (with t the thickness and w the width of the beam cross-section), z the position along the beam's length, P represents the distributed load, and finally, L is the length of the beam. The total beam elongation resulting from its deformation is obtained by integrating the beam profile along its length.

$$\Delta L = \int_0^L \sqrt{1 + (dy/dz)^2}dz - L. \tag{3}$$

When considering the optical signal travelling in the beam, this physical elongation relates to a change in optical path length and is the primary source of phase-shifting induced when the suspended beam deforms.

In addition, the beam deflection produces stress in the beam, which translates into stress-induced optical phase retardance due to the photoelastic coupling. In order to account for this effect, finite element analysis (FEA) is used. The maximum deflection measured by the optical sensor at the center and mid-length of the double-clamped beam is imposed as a deflection on the FEA model. Afterward, the resulting stress states at each node of the mesh are collected and

Optics EXPRESS

analyzed. The clamped-clamped boundary condition causes both, bending and tensile stresses. As confirmed by FEA, the stress is prevalently in the direction of the beam length, where the combined effect of bending (predominant) and tension accounts for a few MPa. Considering the length of the beam (23 mm long), the stress-induced phase retardance is not completely negligible, albeit smaller than the one induced by the change of path-length. To estimate it, the change in refractive index n due to the stress is integrated along the entire length of the beam:

$$\delta = \int_0^L \Delta n \sqrt{1 + (dy/dz)^2}\, dz. \tag{4}$$

with δ the induced retardance. Assuming $\Delta n = CT^z$, where $C = 3.55 \cdot 10^{-12}$ Pa^{-1} is the stress-optic coefficient for fused silica and T^z is the average stress along the direction of propagation of light, estimated from the FEA model. Note that the stress-state perpendicular to the propagation of light induces a negligible contribution (in the order of 10^{-1} MPa) that we do not consider in what follows.

Let us now compare the experimental data of the modulated intensity signal with our theoretical model that predicts the value of the induced phase shift. We consider the point of maximum deflection and in turn induced-retardance for each different AC voltage. The results are shown in Fig. 5. To convert the measured optical intensity signal into phase shift and then into retardance, we assume that the two arms of the Mach-Zehnder interferometer are balanced (i.e. $I_1 = I_2 = I_0$). Thus, we express the intensity after interference as $I_{tot} = 2I_0\{1+\cos[\varphi(t)]\}$. The phase difference can then be described as $\varphi(t) = \Delta\varphi_{max} \sin(\omega t)$, where $\Delta\varphi_{max}$ is the maximum phase shift induced by the device (i.e. the one corresponding to the maximum deflection of the double-clamped beam) and $\sin(\omega t)$ is the sinusoidal oscillation of the double-clamped beam at its first resonance frequency. For example, with an actuation of 100 V^{dc} and 37.5 V^{ac}, the maximum phase shift is measured to be $\Delta\varphi_{max} \approx 0.84\ \pi$. This value is then converted into a phase retardance of 265 nm by considering the wavelength used (632 nm), which is in good agreement with the value predicted by the analytical model, i.e. 252 nm (see Fig. 5). By increasing the AC driving voltage up to 50 V_{pp}, it is possible to reach values of total induced retardance above 300 nm. This value sets the detectable amplitude range for this specific wavelength, such as no phase wrapping occurs which would lead to signal-interpretation ambiguity. In this particular case, it corresponds to a motion amplitude of ≈ 48 μm and is equivalent to a distributed force of $\approx 5 \cdot 10^{-9}$ N/μm. Such values correspond to an acceleration of 4.64 g. The range can be further increased either by using longer wavelengths or by monitoring phase-wrapping using more sophisticated signal processing as opposed to a simple threshold-detection scheme. In such cases, the ultimate limitation will be the bending strength of the double-clamped beam which is design- and material- dependent. A good agreement between experimental results and the model demonstrates the fairness of the assumptions made above.

To prove the device capability for detecting previous frequency states, two different frequency paths, corresponding to an input signal that would have positive and negative chirp are followed to reach the frequency of 600 Hz (see Fig. 6(a)). When a 50 V-excitation signal is applied, this frequency corresponds to a situation where two possible oscillating states can be found as seen in Fig. 6(b). To test the robustness of these two possible frequency states, three frequency steps of increasing ranges (i.e. +/- 10, 20, 30, 40 and 50 Hz) are applied. The resulting displacements are plotted in the mechanical domain in Fig. 6(c) and in the optical domain in Fig. 6(d). For both states, a stable oscillation condition is observed up to an amplitude of 40 Hz. These two states are therefore metastable over a significant oscillation range, i.e. between 620 and 650 Hz, which defines the frequency range of the sensor for chirp-up/chirp-down sensing for this particular case. In other words, the device once entering one of the two states tends to remain there, until it is subjected to large frequency perturbations (>40 Hz, as seen in point 5A). The jump from one frequency to the other is followed by the device within few tens of milliseconds, as shown from

Optics EXPRESS

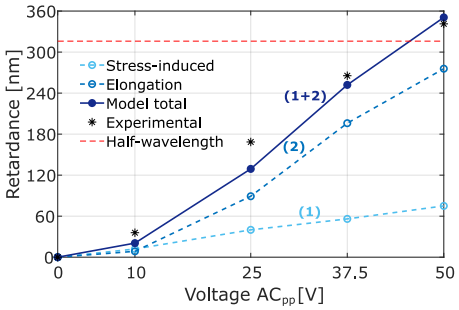

Fig. 5. Induced optical phase retardance and maximum upward deflection versus AC actuating voltage at the resonant frequency (a constant 100 V^{dc} is added). The experimental results (black star) for the maximum optical phase retardance and the model (blue circles), with the contribution from stress and elongation (in turquoise), are represented. Connected lines are shown as a visual aid. Experimental error bars are estimated to be +/- 10 nm.

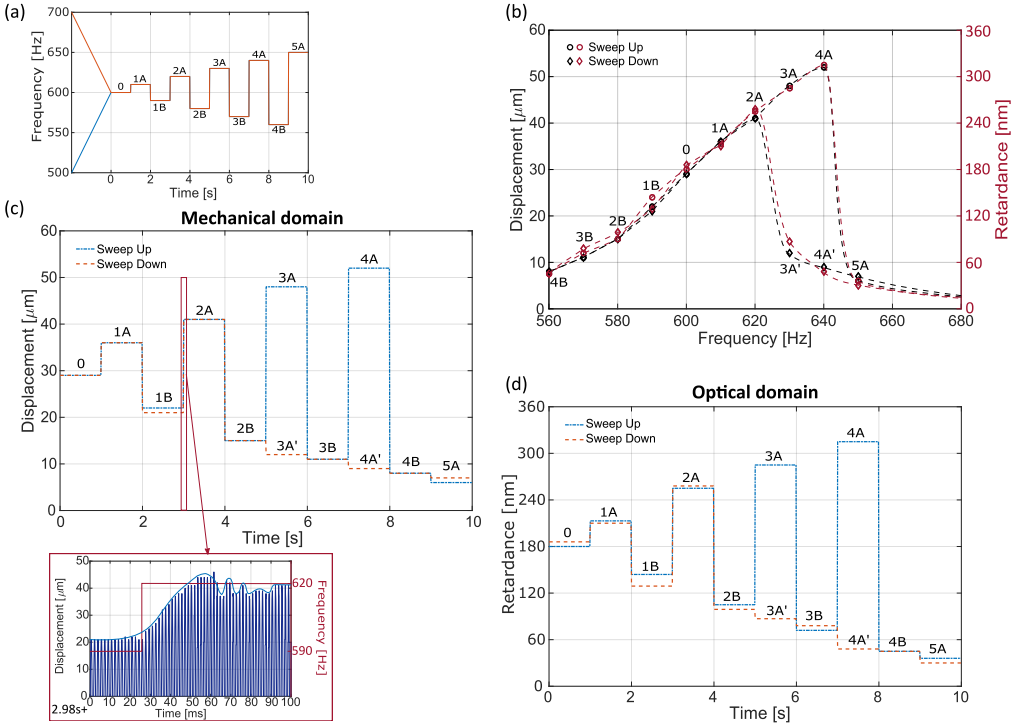

Fig. 6. Bi-stable operation in both mechanical and optical domains. The device is driven at 100 V^{dc} onto which is added an AC voltage of 50 V_{pp}. Two sweeping paths are followed to reach 600 Hz. Subsequently, frequency jumps are performed. (a) Frequency paths followed for the excitation voltage. (b) Experimental values of the measured displacement and retardance at various points in the frequency domain. The dashed curves are shown as a visual aid. (c) and (d) show in the time domain respectively the displacement and the retardance measured while following the frequency paths depicted in (a). A post-process averaging has been performed on the data before plotting. Displacement error measurement is +/- 0.1 µm, while the retardance error measurement is estimated to be +/- 10 nm.

Optics EXPRESS

the inset of Fig. 6(c). We define the response time as the time to reach 95% of the threshold value. Considering Fig. 6(c), the response time for this design is ≈ 20 ms.

This result further demonstrates the coupling of the nonlinearity into the optical domain and the bi-stability of the sensing double-clamped beam. The intensity of the modulated signal can be measured with a photodetector, offering a simple and robust solution to measure the dynamics of the device without any additional sensing means to monitor the beam deflection.

4. Conclusion

We have introduced a concept of optomechanical vibration sensing based on the observation of non-linear vibration states of a suspended waveguide. The working principle is to transduce mechanical vibrations of a double-clamped transparent beam to the optical domain by monitoring the phase shifts of a coherent light signal travelling through the structure. Such a device exhibits an intrinsic non-linear dynamical mechanical response with a characteristic path-dependence with the frequency sweeping direction that can be directly coupled to the optical domain. This effect gives the device the capability of sensing the dynamics of vibrational states, beyond just their amplitude and frequency, and *without* further needs for post-processing of signals. For instance, such a device combined with a simple threshold-intensity detection is able to trigger an alarm not only for excessive vibrations, but furthermore for vibration patterns bearing a positive or even a negative chirp (if laser re-exposure is applied to the beam as described in [8]). The principle is generic and can be adapted to a variety of situations and scales, in particular, thanks to the flexibility of the manufacturing process used to produce the monolithic device. Thanks to its built-in simplicity, this optical sensing principle is notably attractive for remote sensing application in harsh environments as one can remotely separate the all-in-glass sensing element from the light source and the photodetector used to monitor the signal.

Acknowledgment. In this work, E.C., wrote the draft manuscript, implemented the optical modulation concept, modeled it and carried out the experiments, T. Y. designed the proof-of-concept and modelled the DEP actuation and mechanical response, P. V. contributed to the vibration dynamic characterization of the device, Y. B. proposed the initial concept and supervised the research. All authors contributed to the manuscript revisions. The authors further thanks Dr. S. Hakobyan for the fruitful discussions and Dr. J. Gateau for the help in the implementation of the MZI set-up. The Galatea Laboratory acknowledges the sponsoring of Richemont International.

Disclosures. The authors declare no conflicts of interest.

References

1. S. Xu, F. Xing, R. Wang, W. Li, Y. Wang, and X. Wang, "Vibration sensor for the health monitoring of the large rotating machinery: Review and outlook," Sens. Rev. **38**(1), 44–64 (2018).
2. X. Dong, J. Lian, H. Wang, T. Yu, and Y. Zhao, "Structural vibration monitoring and operational modal analysis of offshore wind turbine structure," Ocean Eng. **150**, 280–297 (2018).
3. Y. Zhao, J. Pan, Z. Huang, Y. Miao, J. Jiang, and Z. Wang, "Analysis of vibration monitoring data of an onshore wind turbine under different operational conditions," Eng. Struct. **205**, 110071 (2020).
4. A. Khadka, B. Fick, A. Afshar, M. Tavakoli, and J. Baqersad, "Non-contact vibration monitoring of rotating wind turbines using a semi-autonomous UAV," Mech. Syst. Signal Process. **138**, 106446 (2020).
5. G. Kouroussis, C. Caucheteur, D. Kinet, G. Alexandrou, O. Verlinden, and V. Moeyaert, "Review of Trackside Monitoring Solutions: From Strain Gages to Optical Fibre Sensors," Sensors **15**(8), 20115–20139 (2015).
6. X. Bao and L. Chen, "Recent Progress in Distributed Fiber Optic Sensors," Sensors **12**(7), 8601–8639 (2012).
7. S. Sony, S. Laventure, and A. Sadhu, "A literature review of next-generation smart sensing technology in structural health monitoring," Struct. Control Heal. Monit. **26**, e2321 (2019).
8. O. Abdeljaber, M. Hussein, O. Avci, B. Davis, and P. Reynolds, "A novel video-vibration monitoring system for walking pattern identification on floors," Adv. Eng. Softw. **139**, 102710 (2020).
9. S. Schmid, L. G. Villanueva, and M. L. Roukes, *Fundamentals of Nanomechanical Resonators* (Springer, 2006).
10. S. Shim, M. Imboden, and P. Mohanty, "Synchronized Oscillation in Coupled Nanomechanical Oscillators," Science **316**(5821), 95–99 (2007).
11. D. Antonio, D. H. Zanette, and D. López, "Frequency stabilization in nonlinear micromechanical oscillators," Nat. Commun. **3**(1), 806 (2012).
12. T. Yang and Y. Bellouard, "Laser-Induced Transition between Nonlinear and Linear Resonant Behaviors of a Micromechanical Oscillator," Phys. Rev. Appl. **7**(6), 064002 (2017).

Optics EXPRESS

13. N. Q. Hu and X. S. Wen, "The application of Duffing oscillator in characteristic signal detection of early fault," J. Sound Vib. **268**(5), 917–931 (2003).
14. C. R. Bermúdez-Gómez, R. Enriquez-Caldera, and J. Martínez-Carballido, "Chirp Signal Detection Using The Duffing Oscillator," in *CONIELECOMP* (2012), pp. 344–349.
15. P. Bado, A. A. Said, M. Dungan, T. S. Sosnowski, and S. Wright, "Dramatic Improvements in Waveguide Manufacturing with Femtosecond Lasers," in *NFOEC* (2002), pp. 1153–1158.
16. I. Kovacic and M. J. Brennan, *The Duffing Equation Nonlinear Oscillators and Their Behaviour* (Wiley, 2011).
17. T. Yang and Y. Bellouard, "Monolithic transparent 3D dielectrophoretic micro-actuator fabricated by femtosecond laser," J. Micromech. Microeng. **25**(10), 105009 (2015).
18. Q. P. Unterreithmeier, E. M. Weig, and J. P. Kotthaus, "Universal transduction scheme for nanomechanical systems based on dielectric forces," Nat. Lett. **458**(7241), 1001–1004 (2009).
19. J. Drs, T. Kishi, and Y. Bellouard, "Laser-assisted morphing of complex three dimensional objects," Opt. Express **23**(13), 17355–17366 (2015).
20. K. M. Davis, K. Miura, N. Sugimoto, and K. Hirao, "Writing waveguides in glass with a femtosecond laser," Opt. Lett. **21**(21), 1729 (1996).
21. R. S. Taylor, C. Hnatovsky, and E. Simova, "Ultra-high resolution index of refraction profiles of femtosecond laser modified silica structures," Opt. Express **11**(7), 775–781 (2003).
22. A. A. Said, M. Dugan, and P. Bado, "Waveguide electro-optic modulator in fused silica fabricated by femtosecond laser direct writing and thermal poling," Opt. Lett. **31**(6), 739–741 (2006).
23. A. A. Said, M. Dugan, P. Bado, Y. Bellouard, A. Scott, and J. R. Mabesa Jr., "Manufacturing by laser direct-write of three-dimensional devices containing optical and microfluidic networks," Phot. Process. Microelectron. Photonics III **5339**, 194 (2004).
24. Y. Bellouard, A. A. Said, and P. Bado, "Integrating optics and micro-mechanics in a single substrate: a step toward monolithic integration in fused silica," Opt. Express **13**(17), 6635–6644 (2005).
25. Y. Bellouard, "On the bending strength of fused silica flexures fabricated by ultrafast lasers," Opt. Mater. Express **1**(5), 816–831 (2011).